First principles calculation of lattice thermal conductivity of metals considering phonon-phonon and phonon-electron scattering

Yan Wang, Zexi Lu, and Xiulin Ruan[a)]
School of Mechanical Engineering and the Birck Nanotechnology Center, Purdue University, West Lafayette, Indiana 47907, USA

(Received 18 February 2016; accepted 24 May 2016; published online 14 June 2016)

The effect of phonon-electron (p-e) scattering on lattice thermal conductivity is investigated for Cu, Ag, Au, Al, Pt, and Ni. We evaluate both phonon-phonon (p-p) and p-e scattering rates from first principles and calculate the lattice thermal conductivity (κ_L). It is found that p-e scattering plays an important role in determining the κ_L of Pt and Ni at room temperature, while it has negligible effect on the κ_L of Cu, Ag, Au, and Al. Specifically, the room temperature κ_Ls of Cu, Ag, Au, and Al predicted from density-functional theory calculations with the local density approximation are 16.9, 5.2, 2.6, and 5.8 W/m K, respectively, when only p-p scattering is considered, while it is almost unchanged when p-e scattering is also taken into account. However, the κ_L of Pt and Ni is reduced from 7.1 and 33.2 W/m K to 5.8 and 23.2 W/m K by p-e scattering. Even though Al has quite high electron-phonon coupling constant, a quantity that characterizes the rate of heat transfer from hot electrons to cold phonons in the two-temperature model, p-e scattering is not effective in reducing κ_L owing to the relatively low p-e scattering rates in Al. The difference in the strength of p-e scattering in different metals can be qualitatively understood by checking the amount of electron density of states that is overlapped with the Fermi window. Moreover, κ_L is found to be comparable to the electronic thermal conductivity in Ni. *Published by AIP Publishing.*
[http://dx.doi.org/10.1063/1.4953366]

I. INTRODUCTION

Thermal management is an essential component for the design of modern electronic and photonic devices.[1–3] For example, in heat-assisted magnetic recording devices, the intense photon energy absorbed by plasmons in the near-field-transducer (NFT) is eventually dissipated into the metallic transducer as heat.[2,4] The resulting high lattice temperature could deteriorate the fine structures of the device. Therefore, an accurate modeling of heat transfer processes in the NFT is critical for the design of such devices.[5,6] This is also true for interconnects and heat sinks in electronic devices, where there are usually metallic components in contact with metals, semiconductors, or insulators.

Extensive attention has been paid to the lattice thermal conductivity κ_L of various nonmetals, which has enabled a better understanding of phonon transport in systems composed of semiconductors and insulators.[7–14] However, the κ_L of metals has received much less attention due to the dominance of electronic thermal conductivity in most metals. Recently, the phenomenological two-temperature model (TTM),[15,16] which deals with electron-phonon coupled heat transfer, has been used extensively to interpret experimental observations in thermal metrology of solids and solid-solid interfaces.[17–24] An important implication of the TTM is that the κ_L of metals significantly affects interfacial thermal resistance at metal-dielectric interfaces, of which one component was shown to be proportional to $\kappa_L^{-0.5}$.[21,25–27] Despite that a knowledge of κ_L is required to model thermal transport in such systems involving metallic components, the κ_L of most metals is yet to be fully understood.

Phonon transport in metals is limited by phonon scattering by various sources, for example, phonons, electrons, impurities, and defects, etc. At temperatures comparable to or above the Debye temperature, phonon-phonon (p-p) scattering is believed to dominate phonon relaxation in Cu, Ag, and Au, while phonon-electron (p-e) scattering is neglected.[28] However, it is unclear whether p-e scattering is also negligible in metals known to have much stronger electron-phonon coupling than Cu, Ag, and Au. Several simplified models have been proposed to evaluate this effect in metals and alloys.[29–32] Even though electron density is not the sole factor to determine the electron-phonon coupling constant G_{ep}, it could shed some light on a qualitative estimation of the relative magnitude of G_{ep} in materials. In low-doped semiconductors and insulators, which have very low electron density, phonon scattering by electrons is much rarer than scattering by other phonons at temperatures around or above the Debye temperature.[33] For heavily doped semiconductors, semimetals, and metals, however, the high electron density might lead to a different story. For example, it was reported that p-e scattering could reduce the phonon lifetime significantly in heavily doped silicon.[34] Moreover, it is well known that there is a wide span of G_{ep} in metals.[35] For instance, G_{ep} is on the order of 1×10^{16} W/m^2 K in Cu, Ag, and Au at room temperature, while it is on the order of $1 \times 10^{17} \sim 10^{18}$ W/m^3 K in Al, Pt, and Ni.[35] As the magnitude of G_{ep} characterizes the strength of scattering of electrons by phonons, it is thereby natural to expect that the scattering of phonons by electrons is stronger in Al, Pt, and

a)Electronic mail: ruan@purdue.edu

Ni than in Cu, Ag, and Au. Therefore, an accurate knowledge of κ_L is important for thermal modeling of metal-dielectric systems. Recent advances in first-principles calculations of phonon-phonon, electron-phonon, and phonon-electron scattering rates[8,24,34,36] render it possible to predict the κ_L of metals from first principles. The predicted values can also be used as input parameters in transport equations to study carrier dynamics and thermal non-equilibrium in systems such as ultrafast laser[6,37] and Raman experiments.[24]

In this work, we present first-principles calculations of p-p and p-e scattering rates in Cu, Ag, Au, Al, Pt, and Ni. With these quantities, we are able to compute the κ_L of these metals and evaluate the relative importance of p-p and p-e scattering on κ_L. The rest of this paper is organized as follows. In Sec. II, we present the methodologies for calculating p-p and p-e scattering rates as well as κ_L from first principles. Section III presents the results of scattering rates and κ_L for Cu, Ag, Au, Al, Pt, and Ni. Section IV concludes this paper. The predicted κ_L values have been used as input parameters for Boltzmann equations in our another study[6] on hot electron cooling dynamics under pulsed laser excitation as well as interfacial thermal transport in metal-nonmetal heterojunctions. It should also be noted that during the review of the current paper, it came to our attention that first-principles calculations have also been done on Al, Ag, and Au.[38]

II. METHODOLOGY

A phonon is a quantum of lattice vibration and can be described with a quantum number $\lambda = (\nu, \mathbf{q})$, where ν denotes the branch index and $\mathbf{q}$ denotes the wave vector of a phonon mode. A phonon can be scattered through interaction with other phonons, electrons, impurities, etc. The overall scattering rate of a phonon mode can be estimated by the Matthiessen's rule as $\gamma_\lambda = \gamma_\lambda^{pp} + \gamma_\lambda^{pe} + \gamma_\lambda^{im} + \gamma_\lambda^{gb} ...$, where γ_λ^{pp}, γ_λ^{pe}, and γ_λ^{im} are scattering rates for p-p scattering, p-e scattering, and phonon-impurity scattering, respectively. Since polycrystalline materials are used in many applications,[39,40] grain-boundary scattering of phonons (γ_λ^{gb}) might also be important. In this work, γ^{pp} and γ^{pe} will be calculated from first principles, of which the details are discussed in this section.

A. Phonon-phonon scattering

The p-p scattering contribution (three-phonon process only) to γ_λ is given by the Fermi's golden rule (FGR) as[7,41]

$$\gamma_\lambda^{pp} = \frac{\hbar\pi}{4N}\sum_{\lambda_1\lambda_2}^{+} 2\frac{n_1 - n_2}{\omega\omega_1\omega_2}|V^{+}_{\lambda\lambda_1\lambda_2}|^2\delta(\omega + \omega_1 - \omega_2) + \frac{\hbar\pi}{8N}\sum_{\lambda_1\lambda_2}^{-}\frac{n_1 + n_2 + 1}{\omega\omega_1\omega_2}|V^{-}_{\lambda\lambda_1\lambda_2}|^2\delta(\omega - \omega_1 - \omega_2), \quad (1)$$

where the first term on the right hand side is for phonon absorption (two phonons combine into one), while the second term is for phonon emission (one phonon splits into two). In addition, N is the number of discrete $\mathbf{q}$ points of the Γ-centered $\mathbf{q}$ grid for sampling the first Brillouin zone (FBZ), $\hbar$ is the reduced Planck's constant, n is the Bose-Einstein distribution function, and ω is the phonon frequency. The summation $\sum^{\pm}$ runs over phonon modes and requires conservation of quasimomentum: $\mathbf{q}_2 = \mathbf{q} \pm \mathbf{q}_1 + \mathbf{Q}$, in which $\mathbf{Q}$ is the reciprocal lattice vector with $\mathbf{Q} = 0$ denoting normal process and $\mathbf{Q} \neq 0$ denoting Umklapp process. δ is the Dirac delta function, which is approximated by a Gaussian or Lorentzian function in practice.[42,43] The terms $V^{\pm}_{\lambda\lambda_1\lambda_2}$ are the scattering matrix elements, which are calculated as[7,44]

$$V^{\pm}_{\lambda\lambda_1\lambda_2} = \sum_{l_1}^{N_b}\sum_{l_2,l_3}^{N,N}\sum_{\alpha_1\alpha_2\alpha_3}^{3,3,3}\frac{\partial^3 \mathrm{E}}{\partial r_{l_1}^{\alpha_1}\partial r_{l_2}^{\alpha_2}\partial r_{l_3}^{\alpha_3}}\frac{e_\lambda^{\alpha_1}(l_1)e_{j_1,\pm\mathbf{q}_1}^{\alpha_2}(l_2)e_{j_2,-\mathbf{q}_2}^{\alpha_3}(l_3)}{\sqrt{m_{l_1}m_{l_2}m_{l_3}}}, \quad (2)$$

where m is the atomic mass and $e_{\nu,\mathbf{q}}$ is the normalized eigenvector of the phonon mode $\lambda = (\nu, \mathbf{q})$. In Eq. (2), l_1, l_2, and l_3 run over atomic indices (l_1 runs over only the atoms in the center unit cell, which contains N_b basis atoms), and α_1, α_2, and α_3 represent Cartesian coordinates. The third-order partial derivative is the anharmonic interatomic force constant (IFC) obtained from first principles, in which E is the total energy of the whole system and $r_{l_1}^{\alpha_1}$ denotes the α_1 component of the displacement of atom l_1.

In addition to the third-order IFCs for Eq. (2), one also needs the eigenvalues and eigenvectors of phonon modes to compute γ_λ^{pp} based on Eqs. (1) and (2). The eigenvalues and eigenvectors are obtained from lattice dynamics calculations that require second-order IFCs. In this work, the second-order IFCs are obtained through Fourier transforming reciprocal-space dynamical matrices calculated from the linear-response theory, which is implemented in Quantum ESPRESSO.[45,46] Force constants obtained in this way suffers less error due to long-range interactions than another widely used method, the small-displacement method.[47] The third-order IFCs are obtained through a finite-difference supercell approach, in which Quantum Espresso is used to compute the forces for a minimal set of displaced supercell configurations.

In all the density-functional theory (DFT) calculations within Quantum ESPRESSO, the Troullier-Martins norm-conserving pseudopotentials[48] are used. DFT calculations for the second-order IFCs are conducted with a $\mathbf{k}$-space sampling and integration on a $24 \times 24 \times 24$ Monkhorst-Pack grid and an energy cut-off of E_{cut} for the truncation of the plane wave basis set. E_{cut} is set to be 100 Ry for Cu, Ag, and Au and 120 Ry for Al, Pt, and Ni. In all cases, a Marzari-Vanderbilt cold smearing of 0.02 Ry is used to speed up the convergence of the self-consistent calculations. A $\mathbf{q}$-grid with $5 \times 5 \times 5$ $\mathbf{q}$ points is used for Cu, Ag, and Ag, while a denser $\mathbf{q}$-grid of $16 \times 16 \times 16$ is used for Al, Pt, and Ni. The convergence of phonon dispersion with respect to $\mathbf{k}$-grid density, $\mathbf{q}$-grid density, energy cut-off, and smearing energy has been carefully checked, and the aforementioned values of these parameters ensure convergence within about 2% on phonon frequencies at Γ and X points and less than 0.001 Ry/atom difference in energy. DFT calculations for third-order IFCs are performed on supercells containing $4 \times 4 \times 4$

primitive unit cells. A Γ-point algorithm in Quantum ESPRESSO is used for Cu, Ag, and Au for efficient DFT calculation, while a $3 \times 3 \times 3$ **k**-grid is used for Al, Pt, and Ni.

Two types of exchange-correlation functionals are used, i.e., Generalized Gradient Approximation (GGA)[49] and Local Density Approximation (LDA).[50] Generally speaking, LDA tends to overestimate bonding energies and underestimate bond lengths, and vice versa for GGA. Since the harmonic and anharmonic IFCs are derivatives of the energy, as a general rule, both sets of constants will be larger in magnitude when computed using the LDA. Accordingly, phonon frequencies and scattering rates are usually overestimated by LDA while underestimated by GGA. This, however, might lead to a fictitious cancellation of error for the prediction of thermal conductivity,[42] which is positively correlated to phonon frequencies (heat capacity) while negatively correlated to scattering rates. Finally, the second-order and third-order IFCs are passed to ShengBTE[42] to obtain γ_λ^{pp} on a $16 \times 16 \times 16$ **q**-grid.

B. Phonon-electron scattering

The phonon-electron scattering rate from the FGR is computed as[41]

$$\gamma_\lambda^{pe} = \frac{2\pi}{\hbar} \sum_{\mathbf{k},i,j} |g^\lambda_{j\mathbf{k}+\mathbf{q},i\mathbf{k}})|^2 \times [f_{i\mathbf{k}}(1-f_{j\mathbf{k}+\mathbf{q}})n_\lambda \delta(\epsilon_{i\mathbf{k}} - \epsilon_{j\mathbf{k}+\mathbf{q}} + \hbar\omega_\lambda) - f_{i\mathbf{k}}(1-f_{j\mathbf{k}-\mathbf{q}})(n_\lambda+1)\delta(\epsilon_{i\mathbf{k}} - \epsilon_{j\mathbf{k}-\mathbf{q}} - \hbar\omega_\lambda)], \quad (3)$$

where g is the electron-phonon matrix element, f is the Fermi-Dirac distribution function, **k** is the electron wavevector, i and j are electron band indices, ϵ is the electron energy, and ω is the phonon frequency. The electron-phonon matrix element is calculated as

$$g^\lambda_{j\mathbf{k}+\mathbf{q},i\mathbf{k}} = \sqrt{\frac{\hbar}{2\omega_\lambda}} \langle \psi_{j\mathbf{k}+\mathbf{q}} | \partial U_\lambda | \psi_{i\mathbf{k}} \rangle, \quad (4)$$

which describes the transition of an electron at a Bloch state $i\mathbf{k}$ into another state at $i\mathbf{k}+\mathbf{q}$ by a phonon at state $\lambda = (\nu, \mathbf{q})$. In Eq. (4), ψ is a ground-state Bloch wavefunction and U is the self-consistent Kohn-Sham potential felt by electrons, which depends on the atomic positions. ∂U_λ denotes the first-order derivative of the Kohn-Sham potential with respect to phonon displacement. Details regarding this quantity can be found in literature.[36,51]

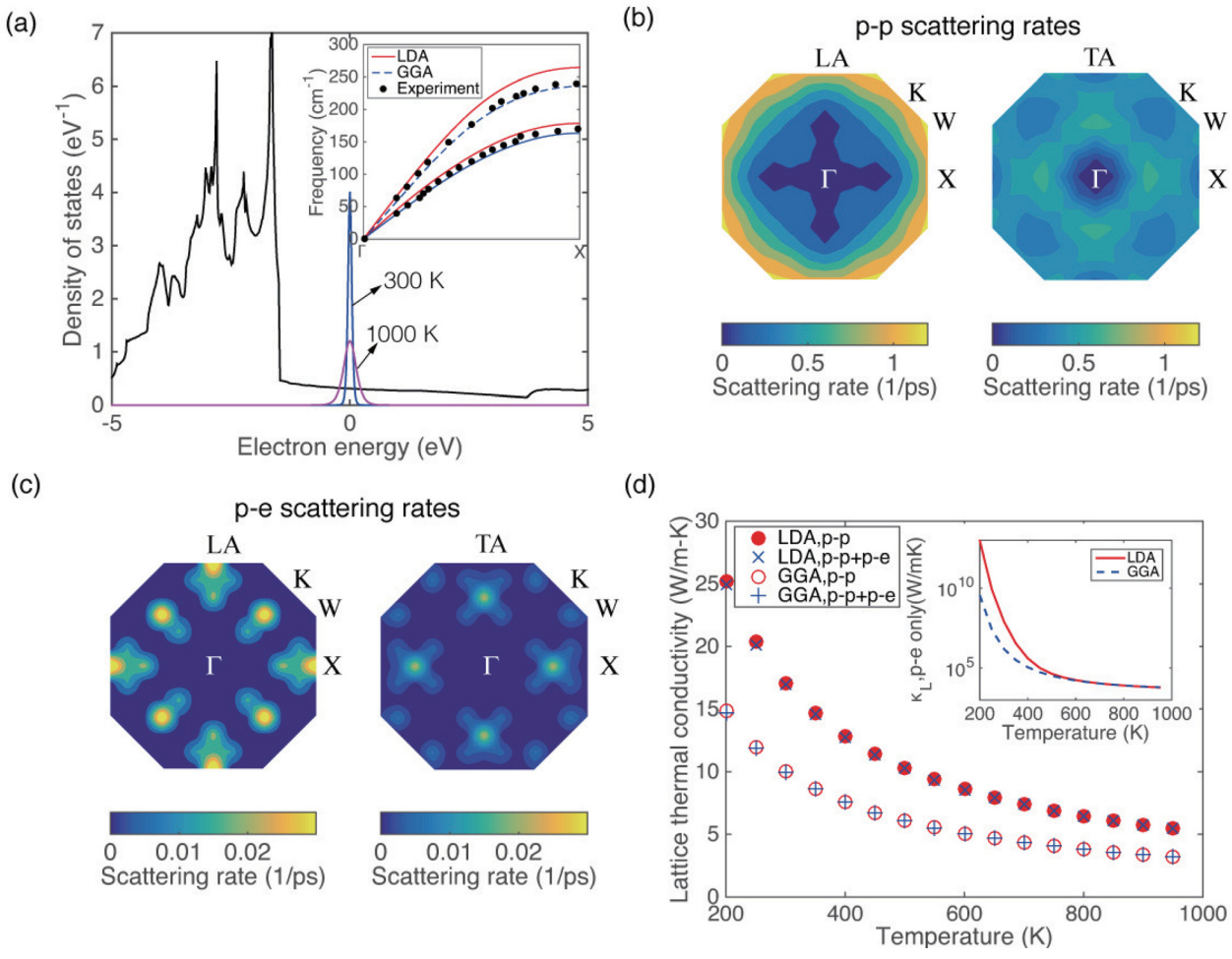

FIG. 1. Results for Cu. (a) Electronic density of states as well as the Fermi window at 300 K and 1000 K. All data in this panel and below are obtained under the GGA approximation otherwise mentioned. The inset shows the phonon dispersion relations calculated in this work as well as experimental data.[62] (b) and (c) Contour plot of the p-p and p-e scattering rates in the k_x-k_y plane of the FBZ. (d) Lattice thermal conductivity computed from first principles with the LDA and GGA approximations with and without the effect of p-e scattering. The inset shows κ_L when only p-e scattering is considered.

Under the relaxation time approximation, the scattering rate (inverse lifetime) of phonon mode λ is[52]

$$\gamma_\lambda^{pe} = \frac{1}{\tau_\lambda^{ep}} = \frac{2\pi}{\hbar}\sum_{\mathbf{k},i,j} |g^\lambda_{j\mathbf{k}+\mathbf{q},i\mathbf{k})}|^2 [f_{i\mathbf{k}} - f_{j\mathbf{k}+\mathbf{q}}] \times \delta(\epsilon_{i\mathbf{k}} - \epsilon_{j\mathbf{k}+\mathbf{q}} + \hbar\omega_\lambda). \quad (5)$$

As we can see, the rate for the scattering of a phonon by electrons only depends on the number of electron states available under the relaxation time approximation, while phonon distribution n is not present in Eq. (5).

Since the energy span of phonons is much smaller than that of electrons, Eq. (5) can be approximated as

$$\gamma_\lambda^{pe} \approx 2\pi\omega_\lambda \sum_{\mathbf{k},i,j} |g^\lambda_{j\mathbf{k}+\mathbf{q},i\mathbf{k})}|^2 \frac{\partial f(\epsilon_{i\mathbf{k}}, T)}{\partial \epsilon} \times \delta(\epsilon_{i\mathbf{k}} - \epsilon_{j\mathbf{k}+\mathbf{q}} + \hbar\omega_\lambda), \quad (6)$$

where $\partial f/\partial\epsilon$ is a "Fermi window" that peaks at the Fermi level. An important property of this function is that it broadens as temperature increases with its integral over the full ϵ-space always being unity. In other words, p-e scattering rate is essentially a weighted average of p-e scattering matrix elements for electron states near the Fermi surface that satisfy energy conservation enforced by the Dirac delta function. Eq. (6) indicates that in order to have low/high p-e scattering rates, the metal should have small/large scattering matrix element g and low/high electron density of states (eDOS) in the Fermi window.

The electron-phonon matrix elements are calculated using ABINIT[53] using the same Troullier-Martins normconserving pseudopotentials as those for IFC calculations. The electron-phonon matrix elements are evaluated on a $16\times16\times16$ **k**-grid and a $16\times16\times16$ **q**-grid. In fact, even with a coarser $12\times12\times12$ **k**-grid and a $12\times12\times12$ **q**-grid, the values of γ^{pe} differ by no more than 5% in most cases, which suggests the values of γ^{pe} obtained on the $16\times16\times16$ **k**-grid and **q**-grid pair should be well converged.

C. Lattice thermal conductivity

Finally, the lattice thermal conductivity tensor can be calculated as

$$\kappa_{L,\alpha\beta} = \sum_\lambda c_{v,\lambda} v_{\lambda,\alpha} v_{\lambda,\beta} \tau_\lambda, \quad (7)$$

where

$$\frac{1}{\tau_\lambda} = \frac{1}{\tau_{\lambda,pp}} + \frac{1}{\tau_{\lambda,pe}}, \quad (8)$$

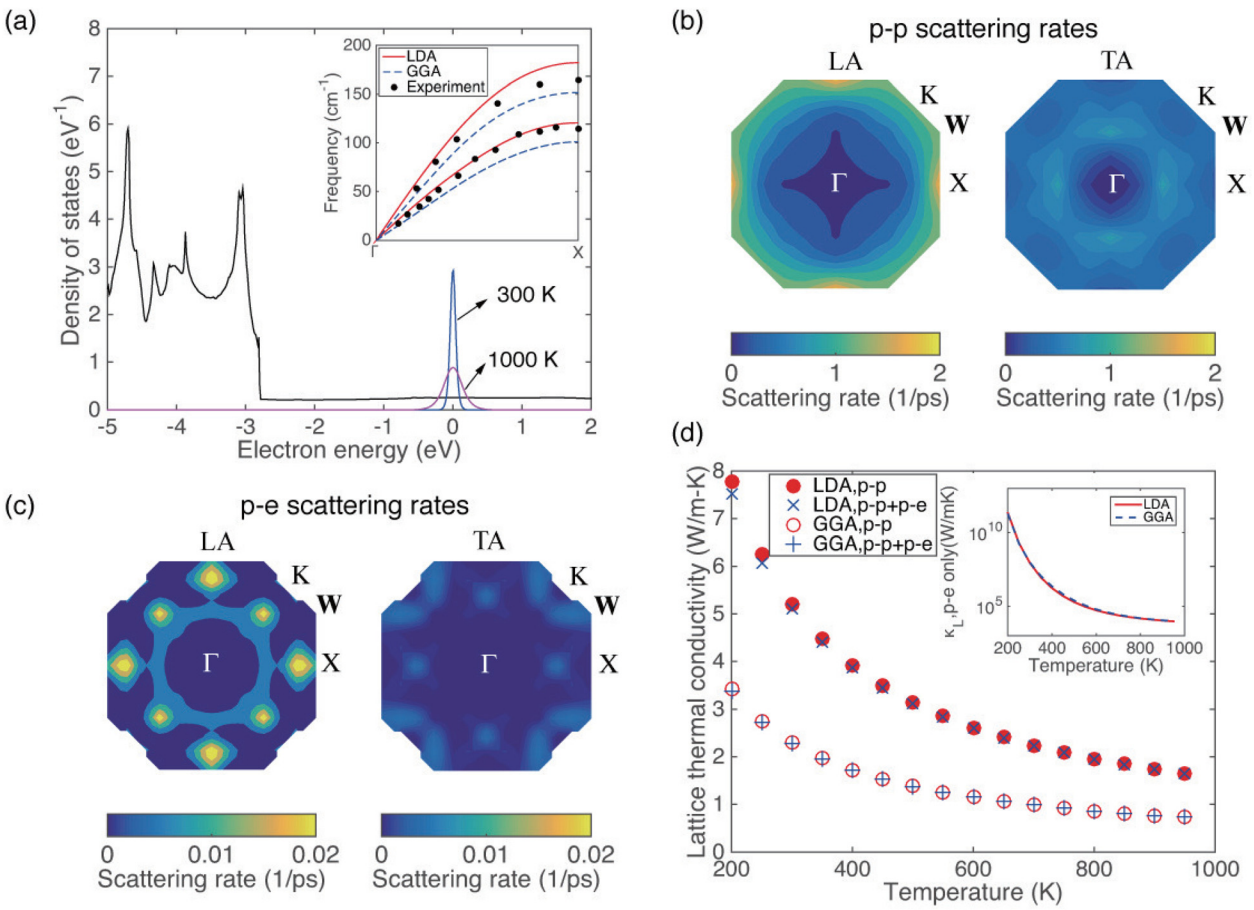

FIG. 2. Results for Ag. (a) Electronic density of states as well as the Fermi window at 300 K and 1000 K. All calculations are obtained under the LDA approximation otherwise mentioned. The inset shows the phonon dispersion relations in the Γ-X direction in the FBZ calculated in this work as well as experimental data.[63] (b) and (c) Contour plot of γ^{pp} and γ^{pe} in the k_x-k_y plane of the FBZ of Ag. (d) κ_L with and without the effect of electron-phonon scattering. The inset shows κ_L when only p-e scattering is considered.

in which the Matthiessen's rule should be applied to individual phonon modes separately.[54] $c_{v,\lambda}$ is the volumetric specific heat of a phonon mode λ and is calculated as

$$c_{v,\lambda} = \frac{1}{k_B T^2} (\hbar\omega_\lambda)^2 n_\lambda (n_\lambda + 1), \tag{9}$$

where k_B is the Boltzmann constant.

Since it is almost impossible to verify our calculations on p-p and p-e scatterings directly, we will compare our results of lattice constants a, phonon dispersion relations, and electron-phonon coupling parameter λ^{ep}, which is also referred to as the mass enhancement factor, with literature values. The phonon dispersions are presented in Figs. 1–5, and λ^{ep}s are calculated using the formalism described in Ref. 56 and listed in Table I. We can see that the calculated λ^{ep} generally falls in the range of literature values. This means that our calculation can at least capture electron-phonon interactions near the Fermi surface with reasonable accuracy.

It is worth noting that, since GGA considers the gradient of the charge density at each position, it generally works better for molecules in which there are abrupt charge density changes with respect to position, whereas LDA works better for metallic systems.[61] However, we will see that GGA results agree better with experimental data of lattice constant, phonon dispersion relations, and electron-phonon mass enhancement factor than LDA for certain metals. Therefore, in this work, we present the results from both LDA and GGA approximations.

III. RESULTS AND DISCUSSIONS

A. Cu, Ag, and Au: Noble metals with weak electron-phonon interaction

Cu, Ag, and Au are noble metals sharing several attributes such as low electrical resistivity and high ductility. All three metals have a single s-orbital electron on top of a fully filled d-orbital electron shell. As a result, the Fermi level of Cu, Ag, and Au lies on the s-band, which has low eDOS, as shown in Figs. 1(a), 2(a), and 3(a). This, as discussed in Ref. 35, leads to a low G_{ep}, which characterizes how fast the thermal energy in hot electrons can be transferred into phonons in the material.[35] Moreover, the s-bands of these metals are rather flat and the d-bands are well below the Fermi level, and even the Fermi window for 1000 K shown in Figs. 1(a), 2(a), and 3(a) has no visible overlap with the d-bands, which suggests insignificant change in electron-phonon interactions

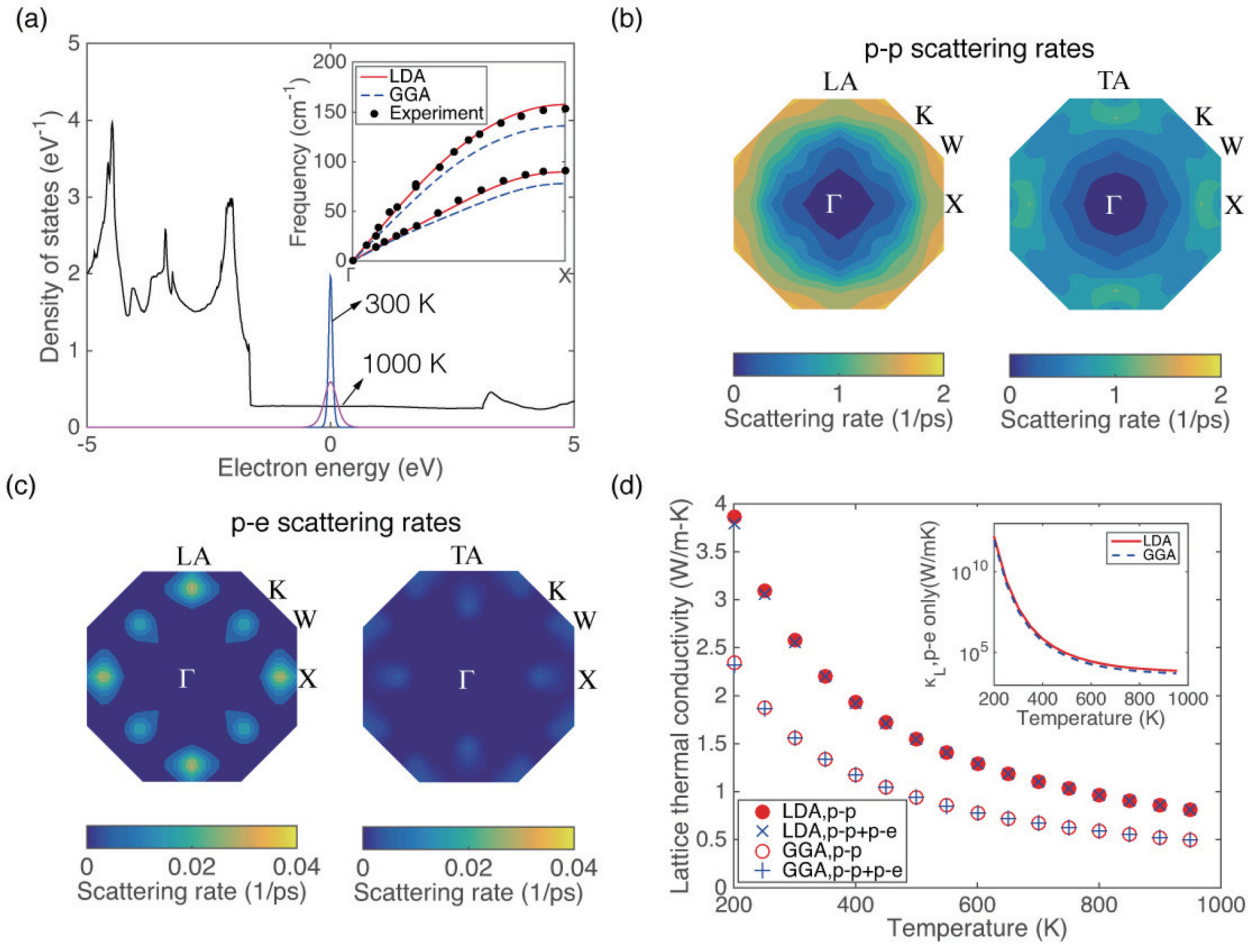

FIG. 3. Results for Au. (a) Electronic density of states as well as the Fermi window at 300 K and 1000 K. All calculations are obtained under the LDA approximation otherwise mentioned. The inset shows the phonon dispersion relations calculated in this work as well as experimental data.[64] (b) and (c) Contour plot of γ^{pp} and γ^{pe} in the k_x-k_y plane of the FBZ. (d) κ_L with and without the effect of electron-phonon scattering. The inset shows κ_L when only p-e scattering is considered.

below 1000 K. Since they have low g and low eDOS in the Fermi window, these metals are expected to have low p-e scattering rates, according to Eq. (6).

The phonon dispersion relations of Cu, Ag, and Au in the Γ-X direction in the FBZ calculated in this work as well as experimental data[62–64] are shown in the inset of Figs. 1(a), 2(a), and 3(a). As we can see, GGA predicts better phonon dispersion relations for Cu, while LDA works better for Ag and Au. Specifically, the frequency of the longitudinal acoustic (LA) branch of Cu is overestimated by LDA, while the frequency of both the LA and transverse acoustic (TA) branches of Ag and Au is underestimated by GGA, which agrees with the previous DFT calculations.[28] Figures 1(b) and 1(c) show the room-temperature p-p and p-e scattering rates, or, γ^{pp} and γ^{pe}, in the k_x–k_y plane of the FBZ. γ^{pp} is on the order of 1 ps^{-1}, similar to that of Si,[8] while γ^{pe} is generally two orders of magnitude lower than γ^{pp}. It is worth mentioning that, even with an electron density of $\sim 8.5 \times 10^{22}\,cm^{-3}$, the γ^{pe} of the LA branch of Cu is on the same order of magnitude as the γ^{pe} of the LA phonons and one order of magnitude lower than that of the LO phonons in heavily doped Si with a carrier concentration of $1 \times 10^{21}\,cm^{-3}$.[34] This is also true for Ag and Au, both of which are characterized by weak p-e scattering, as shown in Figs. 2(b), 2(c), 3(b), and 3(c).

We can also see that the γ^{pp}s of Cu, Ag, and Au are on the same order of magnitude. However, since they have very different atomic masses, with Cu the lightest while Au the heaviest, the lattice thermal conductivity κ_L of them differs significantly owing to the difference in phonon group velocities. As shown in Figs. 1(d), 2(d), and 3(d), the κ_L of Cu is the highest among the three metals, while that of Au is the lowest. In all cases, κ_L decreases with temperature due to enhanced p-p scattering. In addition, the κ_L from LDA and GGA can differ by as much as 50% in certain cases. We suggest using the values from GGA for Cu, while those from LDA for Ag and Au, as they predict more accurate phonon dispersions than the other for the corresponding material. Finally, it is clear from these figures that p-e scattering is negligible in terms of the κ_L of Cu, Ag, and Au at temperature above 200 K, which agrees with previous work on Ag and Au.[38] It is worth mentioning that Makinson's model[30] predicts a converged κ_L in the high-temperature limit when only p-e scattering is considered, while Ziman's model[32] predicts a diverged κ_L. In our work, which considers detailed

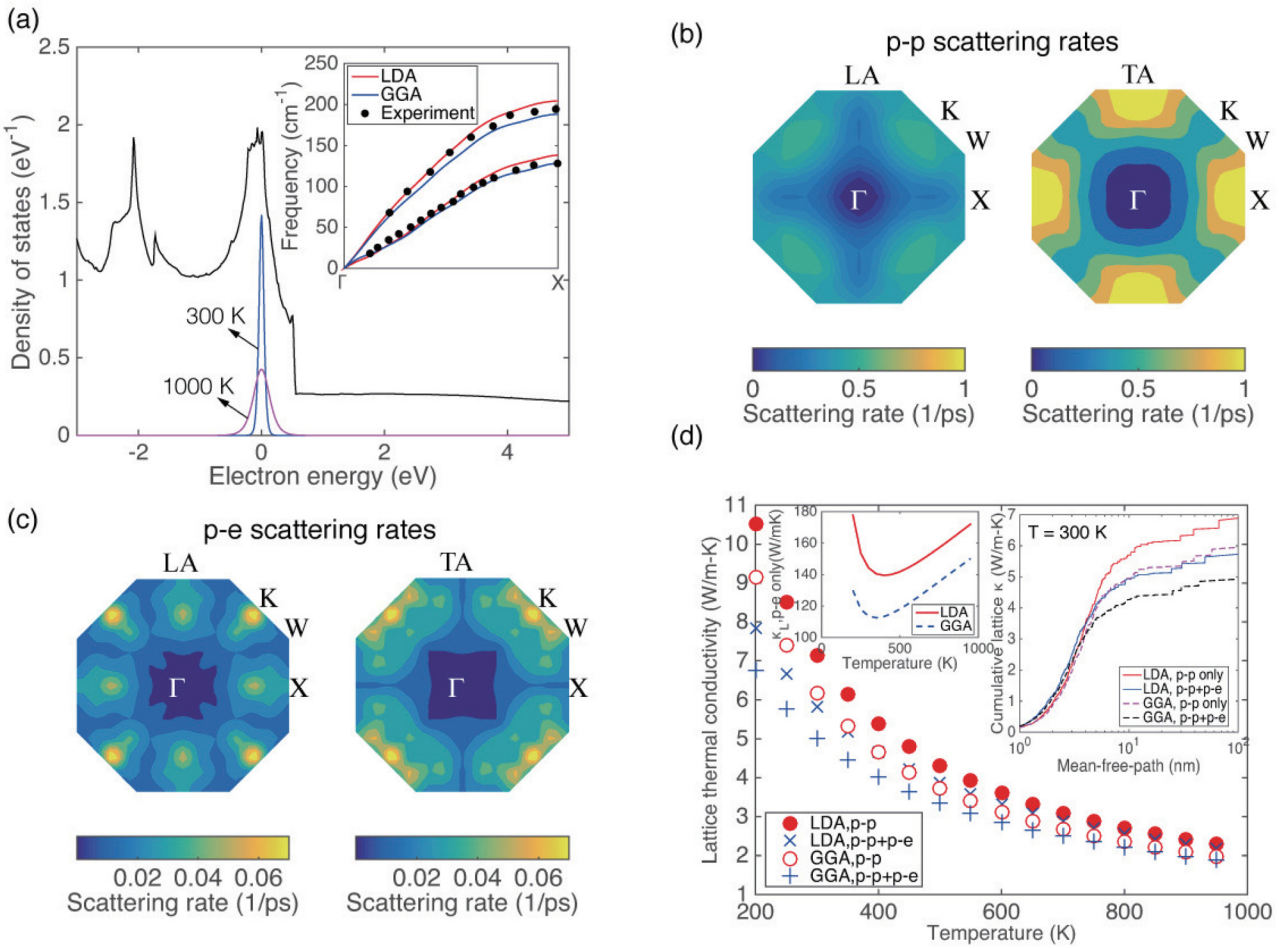

FIG. 4. Results for Pt. (a) Electronic density of states as well as the Fermi window at 300 K and 1000 K. All calculations are obtained under the LDA approximation otherwise mentioned. The inset shows the phonon dispersion relations calculated in this work as well as experimental data (dark symbols).[65] (b) and (c) Contour plot of γ^{pp} and γ^{pe} in the k_x-k_y plane of the FBZ. (d) κ_L with and without the effect of electron-phonon scattering. The inset at the upper left corner shows κ_L when only p-e scattering is considered, and the inset at the upper right corner shows the cumulative thermal conductivity with respect to phonon mean-free-path at 300 K.

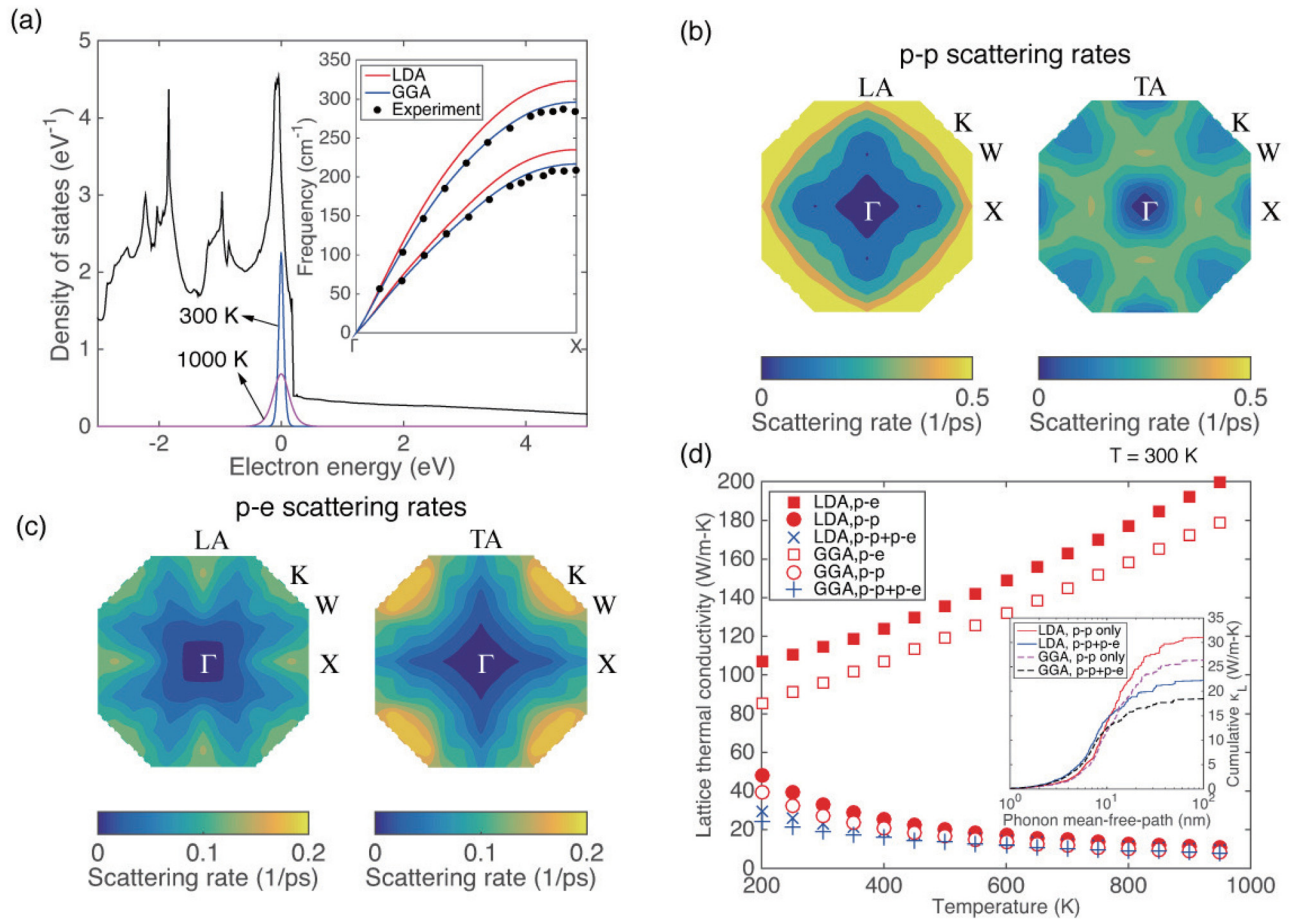

FIG. 5. Results for Ni. (a) Electronic density of states as well as the Fermi window at 300 K and 1000 K. All calculations are obtained under the GGA approximation otherwise mentioned. The inset shows the phonon dispersion relations calculated in this work as well as experimental data (dark symbols).[66] (b) and (c) Contour plot of γ^{pp} and γ^{pe} in the k_x-k_y plane of the FBZ. (d) κ_L considering p-e scattering only, p-p scattering only, and both p-e and p-p scattering. The inset shows the cumulative thermal conductivity with respect to phonon mean-free-path at 300 K.

electronic band structure near the Fermi surface, κ_L is found to decrease with increasing T between 200 and 900 K for Cu, Ag, and Au.

B. Pt and Ni: d-band metals with strong electron-phonon interaction

Pt and Ni are d-band metals, which are characterized by a Fermi level located at the d-band (overlapped with s-band and p-band) with high eDOS. Therefore, e-p interaction can be very strong in these materials, since there are many electron states available for e-p scattering. The strong e-p interaction is manifested by a high e-p coupling constant G_{ep} on the order of 10^{18} W/m^3 K at room temperature, which is two orders of magnitude higher than that of Cu, Ag, and Au.[35]

Figure 4(a) shows the eDOS of Pt, in which the Fermi level is located at the d-band. Evidently, the eDOS at the Fermi level for Pt is much higher than that for Cu, Ag, and Au in Figs. 1(a), 2(a), and 3(a). The inset of Fig. 4(a) shows the phonon dispersion relations. As we can see, LDA predicts more accurate phonon dispersion relations for Pt than GGA.

Figures 4(b) and 4(c) show the γ^{pp} and γ^{pe} of Pt. γ^{pe} is roughly on the same order of magnitude as, though still

TABLE I. Material properties of Cu, Ag, Au, Al, Pt, and Ni. The 2nd column is the electron configuration of these elements. Columns 3 and 4 are the lattice constants calculated through structural relaxation in this work using LDA and GGA, respectively, while column 5 shows the experimental data. The numbers in the parentheses are $(a - a_{\text{exp.}})/a_{\text{exp.}}$. Columns 6 and 7 are the electron-phonon mass enhancement parameter (λ^{ep}) calculated in this work using LDA and GGA, respectively, and column 8 lists the data from literature.

Material	e$^-$ configuration	a_{LDA} (Å)	a_{GGA} (Å)	$a_{\text{exp.}}$ (Å)	$\lambda^{ep}_{\text{LDA}}$	$\lambda^{ep}_{\text{GGA}}$	$\lambda^{ep}_{\text{literature}}$
Cu	$[\text{Ar}]3d^{10}4s^1$	3.668 (+1.61%)	3.553 (−1.58%)	3.610	0.138	0.142	0.13,[55] 0.14[56]
Ag	$[\text{Kr}]3d^{10}4s^1$	4.210 (+2.93%)	4.067 (−0.56%)	4.090	0.135	0.160	0.12,[55] 0.16[57]
Au	$[\text{Xe}]3d^{10}4s^1$	4.183 (+2.52%)	4.075 (−0.12%)	4.080	0.189	0.212	0.15,[55] 0.17,[58] 0.21[57]
Al	$[\text{Ne}]3s^23p^1$	4.046 (−0.10%)	3.961 (−2.20%)	4.050	0.377	0.389	0.38,[59] 0.39,[55] 0.42,[60] 0.44[56]
Pt	$[\text{Xe}]4f^{14}5d^96s^1$	3.995 (+1.91%)	3.914 (−0.15%)	3.920	0.559	0.612	0.66[55]
Ni	$[\text{Ar}]4s^23d^8$	3.544 (+0.97%)	3.441 (−2.24%)	3.520	0.239	0.257	0.31[55]

lower than, γ^{pp}. In particular, γ^{pp} is lower near the center of the FBZ, which indicates that p-e scattering is relatively more significant than at the boundary. The inset of Fig. 4(d) displays the cumulative thermal conductivity of Pt with respect to phonon mean-free-path (MFP). As we can see, most of the κ_L is contributed by phonons with MFP in the range of 1–10 nm. Moreover, phonons with longer MFP (>5 nm) are more significantly affected by p-e scattering than those with shorter MFP, since the long-MFP phonons are mostly modes near the FBZ center with relatively weaker p-p scattering. The discrepancies between the κ_L predicted from the LDA and GGA approximations are not as much as those for Cu, Ag, and Au. In particular, the short MFP region of the cumulative thermal conductivity curves agrees with each other very well. In Fig. 4(d), we can see that p-e scattering reduces the κ_L by 15% at room temperature, and it is even more important at sub-room-temperature regime, where Umklapp p-p scattering becomes weaker, while p-e scattering is less affected.

Figure 5(a) shows the eDOS of Ni, which, similar to Pt, has high eDOS at the Fermi level. The inset shows the phonon dispersion curves. Evidently, the results from GGA agree with experimental data much better than those from LDA. Figures 5(b) and 5(c) are γ^{pp} and γ^{pe} of Ni. Similar to Pt, γ^{pp} and γ^{pe} are comparable to each other. In Fig. 5(d), we can see that the p-e scattering reduces κ_L significantly by about 30% at room temperature and is even more important at sub-room-temperatures. The cumulative κ_L curve in the inset of Fig. 5(d) indicates that p-e scattering substantially affects the κ_L of phonon modes with a wide span of MFP, not just limited to long-MFP ones as in Pt. Unlike Cu, Ag, and Au, κ_L increases with T in the high-temperature regime when only p-e scattering is considered, which seems to support Ziman's model.[32] Finally, it is worth mentioning that, considering its total thermal conductivity of 91 W/m K at room temperature, the κ_L of Ni is comparable to the electronic thermal conductivity. This is unlike most metals in which the lattice thermal conductivity is much lower than the electronic part.

C. Al: Metal with intermediate electron-phonon coupling constant

Aluminum, as a prototype of free-electron-like metals, is among the first metals that are studied *ab initio*. The quadratic-shape eDOS shown in Fig. 6(a) is one signature of the free-electron nature of Al. The γ^{pp} and γ^{pe} of Al are shown in Figs. 6(b) and 6(c). A somewhat unexpected feature

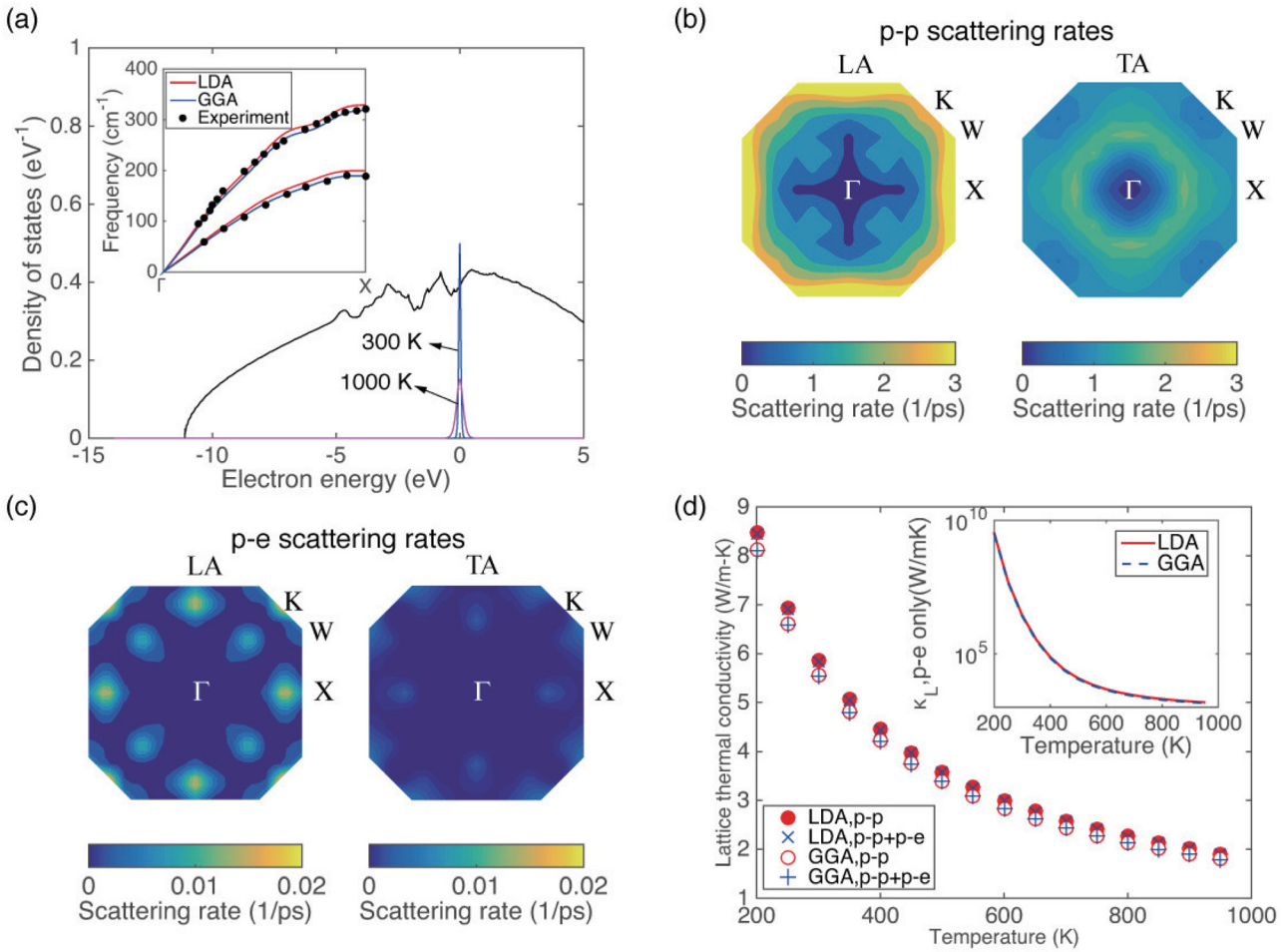

FIG. 6. Results for Al. (a) Electronic density of states as well as the Fermi window at 300 K and 1000 K. All calculations are obtained under the GGA approximation otherwise mentioned. The inset shows the phonon dispersion relations calculated in this work as well as experimental data (dark symbols).[67] (b) and (c) Contour plot of γ^{pp} and γ^{pe} in the k_x-k_y plane of the FBZ. (d) κ_L with and without the effect of electron-phonon scattering. The inset shows κ_L when only p-e scattering is considered.

of the γ^{pe} data is that it is much lower than γ^{pp}, contrary to the common notion that it is a metal with a quite high G_{ep} (for example, $G_{ep} = 2.46 \times 10^{17}$ W/m^3 K at room temperature in Ref. 35). Moreover, Fig. 6(d) shows that p-e scattering has negligible effect on the κ_L of Al, unlike Ni and Pt. It is worth mentioning that in Ref. 38, the calculated p-e scattering rates are higher than this work, which might origin from the different pseudopotentials used for the DFT calculations. In fact, the G_{ep} of Al is about one order of magnitude lower than that of Ni and Pt. A rough estimation of γ^{pe} is G_{ep}/c_p. With c_p similar between Ni, Al, and Pt, the difference in G_{ep} suggests that γ^{pe} should also be much lower in Al than the other two, which agrees with our results. Moreover, the highest γ^{pe} occurs in the high frequency spectrum of phonons (near the boundary of the FBZ), while these phonons only contribute a small amount of heat transfer to the overall κ_L.

IV. CONCLUSION

To conclude, we extracted from first principles the phonon scattering rates in several metals considering the contribution from both p-p and p-e scattering processes. It was found that p-e scattering is negligible in Cu, Ag, Au, and Al, while it is significant in Pt and Ni at room temperature. Specifically, the room temperature κ_L of Cu, Ag, Au, and Al predicted from density-functional theory calculations with the local-density approximation are 16.9, 5.2, 2.6, and 5.8 W/m K, respectively, when only p-p scattering is considered. p-e scattering was found to be negligible in determining κ_L. In contrast, the room-temperature κ_L of Pt and Ni is reduced from 7.1 and 33.2 W/m K to 5.8 and 23.2 W/m K by p-e scattering. Moreover, the effect of p-e scattering on lattice thermal conductivity becomes stronger at sub-room-temperature range.

ACKNOWLEDGMENTS

The authors thank the support from the Defense Advanced Research Projects Agency (Award No. HR0011-15-2-0037).

[1]D. G. Cahill, W. K. Ford, K. E. Goodson, G. D. Mahan, A. Majumdar, H. J. Maris, R. Merlin, and S. R. Phillpot, J. Appl. Phys. **93**, 793 (2003).
[2]W. Challener, C. Peng, A. Itagi, D. Karns, W. Peng, Y. Peng, X. Yang, X. Zhu, N. Gokemeijer, Y.-T. Hsia *et al.*, Nat. photonics **3**, 220 (2009).
[3]D. G. Cahill, P. V. Braun, G. Chen, D. R. Clarke, S. Fan, K. E. Goodson, P. Keblinski, W. P. King, G. D. Mahan, A. Majumdar, H. J. Maris, S. R. Phillpot, E. Pop, and L. Shi, Appl. Phys. Rev. **1**, 011305 (2014).
[4]L. Pan and D. B. Bogy, Nat. Photonics **3**, 189 (2009).
[5]Y. Wang and X. Ruan, in *ASME 2013 Heat Transfer Summer Conference Collocated with the ASME 2013 7th International Conference on Energy Sustainability and the ASME 2013 11th International Conference on Fuel Cell Science, Engineering and Technology* (American Society of Mechanical Engineers, 2013), pp. V001T03A041–V001T03A041.
[6]Y. Wang, Z. Lu, A. K. Roy, and X. Ruan, J. Appl. Phys. **119**, 065103 (2016).
[7]A. Ward, D. Broido, D. A. Stewart, and G. Deinzer, Phys. Rev. B **80**, 125203 (2009).
[8]A. Ward and D. Broido, Phys. Rev. B **81**, 085205 (2010).
[9]Y. Wang, B. Qiu, and X. Ruan, Appl. Phys. Lett. **101**, 013101 (2012).
[10]B. Qiu, Y. Wang, Q. Zhao, and X. Ruan, Appl. Phys. Lett. **100**, 233105 (2012).
[11]T. English, J. Duda, J. Smoyer, D. Jordan, P. Norris, and L. Zhigilei, Phys. Rev. B **85**, 035438 (2012).
[12]Y. Wang, A. K. Vallabhaneni, B. Qiu, and X. Ruan, Nanoscale Microscale Thermophys. Eng. **18**, 155 (2014).
[13]Y. Wang, C. Gu, and X. Ruan, Appl. Phys. Lett. **106**, 073104 (2015).
[14]Y. Wang, H. Huang, and X. Ruan, Phys. Rev. B **90**, 165406 (2014).
[15]M. Kaganov, I. Lifshitz, and L. Tanatarov, Sov. Phys. - JETP **4**, 173 (1957).
[16]S. Anisimov and B. Kapeliovich, Zh. Eksp. Teor. Fiz. **66**, 375 (1974).
[17]W. S. Fann, R. Storz, H. W. K. Tom, and J. Bokor, Phys. Rev. Lett. **68**, 2834 (1992).
[18]T. Q. Qiu and C. L. Tien, J. Heat Transfer **115**, 835 (1993).
[19]C.-K. Sun, F. Vallée, L. Acioli, E. P. Ippen, and J. G. Fujimoto, Phys. Rev. B **48**, 12365 (1993).
[20]D. G. Cahill, K. Goodson, and A. Majumdar, J. Heat Transfer **124**, 223 (2002).
[21]H.-C. Chien, D.-J. Yao, and C.-T. Hsu, Appl. Phys. Lett. **93**, 231910 (2008).
[22]P. E. Hopkins and P. M. Norris, in *Proceedings of the Fifth International Conference on Photo-Excited Processes and Applications (5-ICPEPA)* [Appl. Surf. Sci. **253**, 6289 (2007)].
[23]L. Guo, S. L. Hodson, T. S. Fisher, and X. Xu, J. Heat Transfer **134**, 042402 (2012).
[24]A. K. Vallabhaneni, D. Singh, H. Bao, J. Murthy, and X. Ruan, Phys. Rev. B **93**, 125432 (2016).
[25]A. Majumdar and P. Reddy, Appl. Phys. Lett. **84**, 4768 (2004).
[26]Y. Wang, X. Ruan, and A. K. Roy, Phys. Rev. B **85**, 205311 (2012).
[27]Z. Lu, Y. Wang, and X. Ruan, Phys. Rev. B **93**, 064302 (2016).
[28]X. Tang and B. Fultz, Phys. Rev. B **84**, 054303 (2011).
[29]A. Sommerfeld and H. Bethe, *Electron Theory of Metals* (Julius Springer, Berlin, 1933), p. 450.
[30]R. E. B. Makinson, Math. Proc. Cambridge Philos. Soc. **34**, 474 (1938).
[31]P. Klemens, Aust. J. Phys. **7**, 57 (1954).
[32]J. M. Ziman, Philos. Mag. **1**, 191 (1956).
[33]M. Holland, Phys. Rev. **132**, 2461 (1963).
[34]B. Liao, B. Qiu, J. Zhou, S. Huberman, K. Esfarjani, and G. Chen, Phys. Rev. Lett. **114**, 115901 (2015).
[35]Z. Lin, L. V. Zhigilei, and V. Celli, Phys. Rev. B **77**, 075133 (2008).
[36]B. Qiu, Z. Tian, A. Vallabhaneni, B. Liao, J. M. Mendoza, O. D. Restrepo, X. Ruan, and G. Chen, Europhys. Lett. **109**, 57006 (2015).
[37]Y. Wang and X. Ruan, "A Monte Carlo simulation approach for electron-phonon coupled thermal transport" (unpublished).
[38]A. Jain and A. J. H. McGaughey, Phys. Rev. B **93**, 081206 (2016).
[39]L. Cao, A. Hunter, I. J. Beyerlein, and M. Koslowski, J. Mech. Phys. Solids **78**, 415 (2015).
[40]L. Cao and M. Koslowski, Acta Mater. **61**, 1413 (2013).
[41]J. M. Ziman, *Electrons and Phonons: The Theory of Transport Phenomena in Solids* (Oxford University Press, 1960).
[42]W. Li, J. Carrete, N. A. Katcho, and N. Mingo, Comput. Phys. Commun. **185**, 1747 (2014).
[43]A. J. Ladd, B. Moran, and W. G. Hoover, Phys. Rev. B **34**, 5058 (1986).
[44]G. Deinzer, G. Birner, and D. Strauch, Phys. Rev. B **67**, 144304 (2003).
[45]P. Giannozzi, S. Baroni, N. Bonini, M. Calandra, R. Car, C. Cavazzoni, D. Ceresoli, G. L. Chiarotti, M. Cococcioni, I. Dabo, A. D. Corso, S. de Gironcoli, S. Fabris, G. Fratesi, R. Gebauer, U. Gerstmann, C. Gougoussis, A. Kokalj, M. Lazzeri, L. Martin-Samos, N. Marzari, F. Mauri, R. Mazzarello, S. Paolini, A. Pasquarello, L. Paulatto, C. Sbraccia, S. Scandolo, G. Sclauzero, A. P. Seitsonen, A. Smogunov, P. Umari, and R. M. Wentzcovitch, J. Phys.: Condens. Matter **21**, 395502 (2009).
[46]L. Paulatto, F. Mauri, and M. Lazzeri, Phys. Rev. B **87**, 214303 (2013).
[47]D. Alfè, Comput. Phys. Commun. **180**, 2622 (2009), 40 {YEARS}{OF} CPC: A celebratory issue focused on quality software for high performance, grid and novel computing architectures.
[48]N. Troullier and J. L. Martins, Phys. Rev. B **43**, 1993 (1991).
[49]J. P. Perdew, K. Burke, and M. Ernzerhof, Phys. Rev. Lett. **77**, 3865 (1996).
[50]J. P. Perdew and Y. Wang, Phys. Rev. B **45**, 13244 (1992).
[51]S. Baroni, S. De Gironcoli, A. Dal Corso, and P. Giannozzi, Rev. Mod. Phys. **73**, 515 (2001).
[52]P. B. Allen, Phys. Rev. B **6**, 2577 (1972).
[53]X. Gonze, B. Amadon, P.-M. Anglade, J.-M. Beuken, F. Bottin, P. Boulanger, F. Bruneval, D. Caliste, R. Caracas, M. Côté, T. Deutsch, L. Genovese, P. Ghosez, M. Giantomassi, S. Goedecker, D. Hamann, P. Hermet, F. Jollet, G. Jomard, S. Leroux, M. Mancini, S. Mazevet, M. Oliveira, G. Onida, Y. Pouillon, T. Rangel, G.-M. Rignanese, D. Sangalli, R. Shaltaf, M. Torrent, M. Verstraete, G. Zerah, and J. Zwanziger, Comput. Phys. Commun. **180**, 2582 (2009), 40 {YEARS} {OF} CPC: A

celebratory issue focused on quality software for high performance, grid and novel computing architectures.
[54]T. Feng, B. Qiu, and X. Ruan, Phys. Rev. B **92**, 235206 (2015).
[55]P. B. Allen, Phys. Rev. B **36**, 2920 (1987).
[56]S. Y. Savrasov and D. Y. Savrasov, Phys. Rev. B **54**, 16487 (1996).
[57]R. Hoyt and A. Mota, Solid State Commun. **18**, 139 (1976).
[58]R. Bauer, A. Schmid, P. Pavone, and D. Strauch, Phys. Rev. B **57**, 11276 (1998).
[59]W. L. McMillan, Phys. Rev. **167**, 331 (1968).
[60]E. L. Wolf, *Principles of Electron Tunneling Spectroscopy* (Oxford University Press, 2011).
[61]A. J. Cohen, P. Mori-Sánchez, and W. Yang, Chem. Rev. **112**, 289 (2012).
[62]E. C. Svensson, B. N. Brockhouse, and J. M. Rowe, Phys. Rev. **155**, 619 (1967).
[63]W. Kamitakahara and B. Brockhouse, Phys. Lett. A **29**, 639 (1969).
[64]J. W. Lynn, H. G. Smith, and R. M. Nicklow, Phys. Rev. B **8**, 3493 (1973).
[65]D. Dutton, B. Brockhouse, and A. Miiller, Can. J. Phys. **50**, 2915 (1972).
[66]R. Birgeneau, J. Cordes, G. Dolling, and A. D. B. Woods, Phys. Rev. **136**, A1359 (1964).
[67]R. Stedman and G. Nilsson, Phys. Rev. **145**, 492 (1966).